6. Dean, A. L., Nitrogen and organic matter in Hawaiian pineapple soils. *Soil Sci.*, 1930, **30**, 439–442.
7. Jenny, H., Bingham, F. T. and Padilla-Saravia, B., Nitrogen and organic matter contents of equatorial soils of Colombia, South America. *Soil Sci.*, 1948, **66**, 173–186.
8. Smith, R. M., Samuels, G. and Cernuda, C. F., Organic matter and nitrogen build-ups in some Puerto Rican soil profiles. *Soil Sci.*, 1951, **72**, 408–427.
9. Eswaran, H., Van den Berg, E. and Reich, P., Organic carbon in soils of the world. *Soil Sci. Soc. Am. J.*, 1993, **57**, 192–194.
10. Batjes, N. H., Total carbon and nitrogen in the soils of the world. *Eur. J. Soil Sci.*, 1996, **47**, 151–163.
11. Jones, R. J. A., Hiederer, R., Rusco, E. and Montanarella, L., Estimating organic carbon in the soils of Europe for policy support. *Eur. J. Soil Sci.*, 2005, **56**, 655–671.
12. Bhattacharyya, T., Pal, D. K., Mandal, C. and Velayutham, M., Organic carbon stock in Indian soils and their geographic distribution. *Curr. Sci.*, 2000, **79**, 655–660.
13. Rasmussen, C., Distribution of soil organic and inorganic carbon pools by biome and soil taxa in Arizona. *Soil Sci. Soc. Am. J.*, 2006, **70**, 256–265.
14. Jenny, H. and Raychaudhuri, S. P., *Effect of Climate and Cultivation on Nitrogen and Organic Matter Reserves in Indian Soils*, ICAR, New Delhi, 1960.
15. Wilding, L. P., Factors of soil formation: Contributions to pedology. In *Factors of Soil Formation: A Fiftieth Anniversary Retrospective* (eds Amundson, R., Harden, J. W. and Singer, M. J.), Soil Science Society of America Special Publication No. 33, Madison, USA, 1994, pp. 15–30.
16. Retallack, G. J., The environmental factor approach to the interpretation of paleosols. In *Factors of Soil Formation: A Fiftieth Anniversary Retrospective* (eds Amundson, R., Harden, J. W. and Singer, M. J.), Soil Science Society of America Special Publication No. 33, Madison, USA, 1994, pp. 31–64.
17. Vitousek, P. M., Factors controlling ecosystem structure and function. In *Factors of Soil Formation: A Fiftieth Anniversary Retrospective* (eds Amundson, R., Harden, J. W. and Singer, M. J.), Soil Science Society of America Special Publication No. 33, Madison, USA, 1994, pp. 87–97.
18. Bourgeon, G., *Explanatory Booklet on the Reconnaissance Soil Map of Forest Area: Western Karnataka and Goa*, Institut français de Pondichéry, travaux de la section scientifique et technique, hors série 20, Pondicherry, 1989.
19. Ferry, B., *Les humus forestiers des Ghâts occidentaux en Inde du Sud. Facteurs climatiques, édaphiques et biologiques intervenant dans le stockage de la matière organique du sol*, Institut français de Pondichéry, Pondicherry, 1992.
20. Peterschmitt, E., *Les couvertures ferrallitiques des Ghâts occidentaux en Inde du Sud. Caractères généraux sur l'escarpement et dégradation par hydromorphie sur le revers*, Publication du department d'ecologie no. 32, Institut français de Pondichéry, Pondicherry, 1993.
21. Grewal, K. F., Buchan, G. D. and Sherlock, R. R., A comparison of three methods of organic carbon determination in some New Zealand soils. *J. Soil Sci.*, 1991, **42**, 251–257.
22. Watson, R. T., Noble, I. R., Bolin, B., Ravindranath, N. H., Verardo, D. J. and Dokken, D. J., *Third Assessment Report on Land Use, Land Use Change and Forestry*, A Special Report of the IPCC, Cambridge University Press, UK, 2000.
23. Friedman, J. H., Greedy function approximation: A gradient boosting machine. *Ann. Stat.*, 2001, **29**, 1189–1232.
24. Freund, Y. and Schapire, R. E., Experiments with a new boosting algorithm. In Proceedings of the Thirteenth International Conference on Machine Learning, 1996, pp. 148–156.
25. Breiman, L., Friedman, J. H., Olshen, R. A. and Stone, C. J., *Classification and Regression Trees*, Wadsworth, Pacific Grove, CA, 1984.
26. Friedman, J. H. and Meulman, J. J., Multiple additive regression trees with applications in epidemiology. *Stat. Med.*, 2003, **23**, 1365–1381.
27. Pandey, D. N., Global climate change and carbon management in multifunctional forests. *Curr. Sci.*, 2002, **83**, 593–602.
28. Ravindranath, N. H. and Somashekhar, B. S., Potential and economics of forestry options for carbon sequestration in India. *Biomass and Bioenergy*, 1995, **8**, 323–336.
29. Bhadwal, S. and Singh, R., Carbon sequestration estimates for forestry options under different land-use scenarios in India. *Curr. Sci.*, 2002, **83**, 1380–1386.
30. Pascal, J. P., *Carte des bioclimats des Ghâts occidentaux (1 : 500,000 scale)*, Institut français de Pondichéry, travaux de la section scientifique et technique, hors série 17, Pondicherry, 1982.
31. Geological Survey of India, *Geological and Mineral Map of Karnataka and Goa*, Bangalore, 1981.
32. Pascal, J. P., with the collaboration of Shyam Sunder, S. and Meher Homji, V. M., *Forest Map of South India, Sheets Shimoga and Mercara–Mysore*, Institut français de Pondichéry, Pondicherry, 1982.
33. Pascal, J. P., with the collaboration of Shyam Sunder, S. and Meher Homji, V. M., *Forest Map of South India, Sheets Belgaum–Dharwar–Panaji*, Institut français de Pondichéry, Pondicherry, 1984.
34. Ramesh, B. R., De Franceschi, D. and Pascal, J.-P., *Forest Map of South India, Sheets Coimbatore–Thrissur*, Institut français de Pondichéry, travaux, Pondicherry, 2002.

ACKNOWLEDGEMENTS. Funding for this research was provided by the Indo-French Centre for the Promotion of Advanced Research (Project no. 2909-1).

Received 4 December 2006; revised accepted 26 April 2007

Earthquake patterns based on diurnal and semidiurnal electromagnetic emissions related to earthquakes/volcanoes observed with 24 h periodicity

V. G. Kolvankar

Seismology Division, Bhabha Atomic Research Centre, Trombay, Mumbai 400 085, India

Electromagnetic (EM) emissions related to earthquakes and volcanoes were observed in a very wide frequency band from VLF to microwave. These were found to be diurnal and semidiurnal type occurring only during certain hours of the day. It was also found in these examples that the occurrences of earthquakes/eruption of volcanoes were simultaneous with the timings of these EM emissions. From this study, it can be concluded that the semidiurnal stresses on the earth and on the moon are solely caused by the position of the Sun. The causes of diurnal stresses are not precisely known.

e-mail: vkolvankar@yahoo.com

In order to study the variation of the stresses developed over a longer period of time, the earthquakes for various regions of the globe were mapped for number of years on 24 h basis. The histogram of earthquakes thus generated on 24 h basis (HE24H) provided various patterns. It was observed that most earthquakes were aligned to some curvature representing some kind of stress fronts of different strengths and lasting up to over 100 years. They were also found in different shapes and sizes. The study of HE24H also supports the hypothesis that the occurrence of earthquakes is synchronous to the earth's rotation.

Keywords: Diurnal and semidiurnal type, earthquakes, electromagnetic emissions, volcanoes.

A RADIO telemetered seismic network (RTSN) was set up at Bhatsa (Thane District, Maharashtra, India) to monitor the reservoir-induced seismicity (RIS) of the local region. This network had nine field stations spread over an area of around 500 sq. km. Each station had a single vertical seismometer and frequency-modulated analogue signals were telemetered to the base station via individual links operated at the spot frequency in UHF band (461–462 MHz), on a 24 h basis. Data from this network were edited on-line and the event portion with about 15 s of the pre-event portion was recorded on a magnetic tape in digital format[1].

In the second quarter of 1991, this network recorded an earthquake sequence (swarm) from Valsad region, Gujarat, India. Between 25 March 1991 and 28 June 1991, nearly 400 events in the magnitude range of 1.4 to 5.1 were recorded from this region, situated about 115 km north of the network[2].

This network experienced a unique radio frequency (RF) disturbance in the UHF telemetry links between field stations and the base station before, during and after this earthquake sequence. During 5–11 March 1991, the telemetry links were severely disturbed (diurnal-type) at certain times (at 00.00 GMT/0530 local time) of the day for durations of up to 20 min. After the onset of the earthquake sequence, the RF disturbances observed were of much longer duration, extending over 100 min and were confined to the disturbances of telemetry links from stations situated in the northern region only (in the direction of the source of the Valsad earthquake sequence).

Prior to the main event on 30 April 1991, for about a three-week period, the RF disturbances were confined to twice a day, at around 04 and 12 h (GMT). This semidiurnal-type RF disturbance vanished after the occurrence of the main event. The RF disturbance is discussed in detail elsewhere[2].

It is believed that the RF emissions come directly from the crystalline rocks of the crust. These rocks provide some sort of a piezoelectric effect when subjected to stress. Laboratory tests have been performed to check radio emissions when different samples of rocks are subjected to stress by other workers[3,4].

Several researchers have witnessed semidiurnal-type EM emission related to earthquakes and volcanoes (Table 1). The important features of this semidiurnal-type EM emissions are as follows: (i) The EM emissions related with earthquakes and volcanoes were found in a very wide frequency band from VLF to microwave. Different workers have chosen the frequency of their interest and convenience. (ii) These emissions were equally spaced in timescale (time offset) on either side of the local midday timings. (iii) Occurrences of the earthquakes and volcanoes were simultaneous with these emission timings, indicating clearly that stresses were developed during these timings. (iv) The timings of semidiurnal emission provided different time-offsets (displacements) from the local noontime from ±1.5 to ±5 h.

In general, the EM emissions of semidiurnal-type were associated with the surface of the earth and the moon, and were primarily caused by the sun. This is a daily phenomenon and the rise in intensity of the EM emission, is attributed by the region, which is mature for earthquakes.

Figure 1 shows the starting and ending portions of a typical RF disturbance (diurnal-type) observed at Bhatsa prior to the Valsad earthquake sequence. Portions of different links in Bhatsa net were rearranged in order of their disturbance periods. This provided an envelope of rising and falling emission signals. In this diurnal-type of RF emission, signal strength increased steadily (with increasing stress) knocking down the different links at different times (based upon received signal strength of different station signals). Later when this RF emission signal strength decreased steadily, it brought back the links with higher signal strength first, followed by other links with lower strengths in decreasing order.

It was observed in cases of semidiurnal-type of emissions that the sun could be instrumental in generating the stresses on earth. Similarly, in the case of diurnal type emissions, considering their consistent timings, again some external forces could be responsible for these phenomena. These external forces may possibly be caused by the planetary position. During the entire week, at a certain time of the day, this (Valsad) portion of the globe would see the same planet position. The steady increase and decrease of RF emission could be due to the rotation of the earth, which brought this earthquake region to face a certain planet position and then steadily moved away from it. However, more such examples are needed to confirm the possible causes of diurnal type of emission.

At Bhatsa, the timings of diurnal-type RF emissions (at 00 h GMT) and those of semidiurnal-type (at 0400 and 1200 h GMT) were different. Also the EM emission in diurnal pattern was more intense. In case of the Chilean earthquake of 22 May 1960 (Mb = 9.5), Warwick *et al.*[5] provided the details of radio noise at 18 MHz on 16 May 1960 between 0350 GMT and 0410 GMT, six days prior

Table 1. Details of six examples of semi-diurnal RF emissions, spaced equally from the local noon timings

Earthquake/volcano sequence place–period–frequency–band of EM emission	Timings of semidiurnal EM emissions	Local noontime and time offset of EM emissions	Occurrence of earthquake–volcanic eruption	Remarks
Valsad[2], India 10–30 April 1991 UHF, range 460–461 MHz	0400 GMT (0900 LT) and 1200 GMT (1700 LT) Duration 10–100 min	0800 GMT (1300 IST) Time offset = ± 4 h	04 : 17 (GMT) on 14 April 1991 foreshock; 05 : 13 h (GMT) on 30 April 1991 main shock.	The timings of the main shock and one of the two foreshocks closely matched that of the first RF emission. Semidiurnal-type EM emission seized after the main shock
Mt. Mihara volcano[9], 3–21 November 1986 LF-82 KHz	9–11 h JST 14–16 h JST	1230 h JST Time offset = ± 2.5 h	First eruption at 1725 h JST, (15 November 1986. Second eruption at 1615 h JST, 21 November 1986.	Both eruptions occurred close to the timings of the EM emissions
Chilean earthquake[10] 16–23 May 1960 HF 10 MHz and HF 18 MHz	8–12 h GMT and 19–24 h GMT	1700 h GMT approx. Time offset = ± 5 h	All six earthquakes, with magnitude range of 6.7–9.5 occurred within the timing of RF emission.	These six events consisted of two foreshocks, a main shock and three aftershocks listed in Gokhberg Mikhial *et al.*[10]
ORSOC, Japan[11] 17 July 2001 VHF 76–108 MHz	9–11 h JST 1230–1430 JST	1200 h JST approx. Time offset = ± 1.5 h	Four events occurred within the time period of three days from the occurrence of RF emission. The timings of two of them matched with those of the RF emission.	RF emissions were observed on an array of VHF receivers on 17 July 2001. Four events (NEIC-USGS) occurred within three days of this emission, which lay within ± 4° long. and ± 5° lat. from Okayama Ridai Seismic Observatory Center, Japan.
VLF sub-ionospheric signals (Kobe quake)[12] VLF range 3–23 January 1995 10.2 kHz and 11.3 kHz	0830 h JST and 1630 h JST	Around 12–30 h JST (timings of the VLF phase reaching minimum). Time offset = ± 4.0 h	The timings of the VLF signal phase reaching minimum were spaced equally from the noon local time. Kobe earthquake timings (0546 h) differed by a couple of hours from the first VLF phase minimum timing.	The sub-ionospheric VLF omega signal was transmitted from Tsushima to Inubu. The signal propagation characteristics (phase in particular) exhibited abnormal behaviour (especially around the sunrise and sunset local times) a few days before the main shock of 1995.
Apollo Lunar Seismic data[13] for stations 12 and 16 (1969–77) Microwave range 1–2 GHz	Around 10 and 23 days from new moon (station 12). Around 7 and 20 days from new moon (station 16)	Around 16.5 days from new moon (station 12). Around 13.5 days from new moon (station 16)	The power spectra of the moonquakes provided major peaks corresponding to the sidereal phase and smaller peak corresponding to synodic month, which suggested occurrences of moonquakes during noisy periods[12].	The three days (solar) offset in time of sunrise/sunset for stations 12 s and 16 reflects 39° difference in longitude between the stations. The local noisy periods, around 10 and 23 days for station 12 around 7 and 20 days (from new moon) for station 16, were not simultaneous and varied with longitude.

to the great earthquake. These timings are again different than those of the semidiurnal-type (listed in Table 1). In both cases (Bhatsa and Chilean earthquakes) diurnal-type of emissions led to the semidiurnal-type of emissions.

Both diurnal- and semidiurnal-type of emissions observed at Bhatsa and also observed at other places provide correlation with the rotation of the earth. Occurrences of moonquakes have also provided direct correlation with the rotation of moon. FFT spectra of the moonquakes provide major peaks at 50 and 100% of the sidereal phase (13.6 and 27.2 days)[6]. However, this semi-diurnal RF emission observed on a daily basis does not provide any correlation with the lunar tidal forces, which is considered as another triggering source for earthquakes[7].

In order to observe the variation of stress timing over a longer period, a histogram of earthquakes on a 24 h basis (HE24H) was constructed, with the horizontal axis representing 24 h and with the vertical axis providing periods in years. The earthquakes were plotted on this graph by means of circular dots of relative sizes representing the

magnitude. The colour contrast was also used for earthquakes in different magnitude ranges for ease of identification.

Figure 2 *a* provides HE24H of South East Asia (SEASIA – lat: 20°S–20°N, long: 90°E–135°E) for the 32-year period (1973–2004) for all earthquakes of magnitude 6.5 and above. Colour codes were used for different magnitude ranges, as indicated. A close examination of this HE24H graph indicates that most earthquakes were aligned in multiple curves representing different sets of patterns. Figure 2 *b* provides multiple patterns of curves drawn in different colours around a circular ring of earthquakes with relatively no major earthquake within, which represents the eyes of these patterns. These sets of curves of concentric circles are similar to the mathematical curve of the Cartesian Oval type.

As mentioned earlier, these curves represent the stress fronts exerted at the earthquake regions on a 24 h basis. As seen from Figure 2, each earthquake lies on the cross-section of two or more curves, indicating that the total stress created by these stress fronts at the cross-over points causes these earthquakes. As one could visualize, many such curves can be drawn to cover all the earthquakes. Also, these curves extend beyond the boundaries of the *X*-axis and appear on the other side. To demonstrate this, two such HE24Hs for the same region were combined in Figure 3 and the same sets of curves are illustrated. The arrangement also facilitates drawing more patterns in a single diagram. In Figure 3, the rounded, semi-opaque areas represent the eyes of different sets of patterns. It is observed that there is no higher magnitude earthquake residing within these areas. This feature was observed in most eyes of various patterns. Curves belonging to other patterns passing through these areas would sometime contain earthquakes with lesser magnitude.

Apart from the curves of the Cartesian Oval type, those similar to Half Cardioids (half portion of the mathematical curve type Cardioids) were commonly observed.

Figure 4 illustrates HE24H of the entire globe for $Mb > 7.2$ for the period 1973–2004. Colour codes were provided for earthquakes from different sub-regions of the world, as indicated in Figure 4. Figure 5 illustrates part of this for 00–15 h (*X*-axis), for the years 1973–89 (*Y*-axis). Part A illustrates the raw HE24H for this portion and alignment of two types of curves drawn with sky blue and yellow colours in part B, which can be visualized through naked eye. Parts C–F illustrate HE24H for four major seismic regions of the globe, PPR (Pacific Plate Right, consisting of North and South America), EUMEIC (Europe, Middle East, India China, Taiwan, Korea), AASIA (Africa and South East Asia) and PPL (Pacific Plate Left consisting of Alaska, Japan, Philippines, South East Australia and New Zealand). As illustrated, these regions share the half Cardioids type of curves illustrated in sky blue and yellow colours. It clearly demonstrates, how this type of curve representing stress fronts, acts globally. The detailed patterns for different parts of the globe are illustrated elsewhere[8].

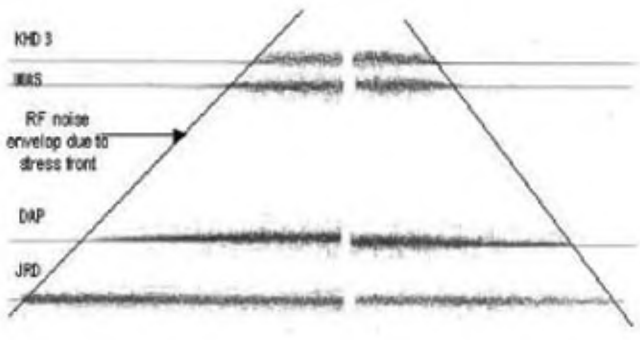

Figure 1. Starting and ending portions of different links in the Bhatsa net rearranged in terms of the received signal strength which provided an envelope of rising and falling RF emission signals.

It has been observed that when the strongest stress front crosses (in HE24H) another similar stress front, it results in an earthquake of magnitude of 7 or more. If more than two such stress fronts pass through a common point, it results in an earthquake of higher magnitude. It is also observed that an earthquake of magnitude 8+ occurs when a number of such stress fronts pass through a common point. It was also noticed that pairs of these higher-magnitude earthquakes were closely spaced in HE24H.

Figure 6 provides HE24H for Alaska region for a 102-year period. There were four big earthquakes of $Mg = 8$ and above. The first pair (A and B) comprises earthquakes during 1964–65, including the second biggest earthquake of the 20th century at Alaska with magnitude of 9.2. Timings of these two quakes are (A) 03 : 36 : 14 on 28 March 1964 ($Mb = 9.2$) and (B) 05 : 01 : 21 on 4 February 1965 ($Mb = 8.7$). Timings of the other pair of earthquakes are (C) 14 : 22 : 31 on 9 March 1957 ($Mb = 8.8$) and (D) 20 : 18 : 41 on 10 December 1938 ($Mb = 8.3$). These two pairs of earthquakes have multiple stress fronts passing through their point of occurrence, as indicated in Figure 6.

The stress fronts indicated in Figure 6 bear shapes similar to magnetic lines of force across the NS poles of a magnet. In this case, these two quakes take the positions of the poles of the magnet. According to the magnetic lines of force, the stress fronts are seen on either side of the positions of these two earthquakes. Similar stress fronts were seen around the other pair of earthquake positions.

Figure 7 shows double HE24H of the same region and extended curves representing stress fronts are displayed. It provides a clear picture of the number of stress fronts passing through the positions of these two earthquakes. Similar extended stress fronts were seen around the other pair of earthquake positions.

Multiple stress fronts were also seen between most of the stronger earthquakes on the HE24H when taken in pairs. Figure 8 shows the histogram (HE24H) for Pacific Plate Right (PPR) region for a 30-year (1973–2002) period.

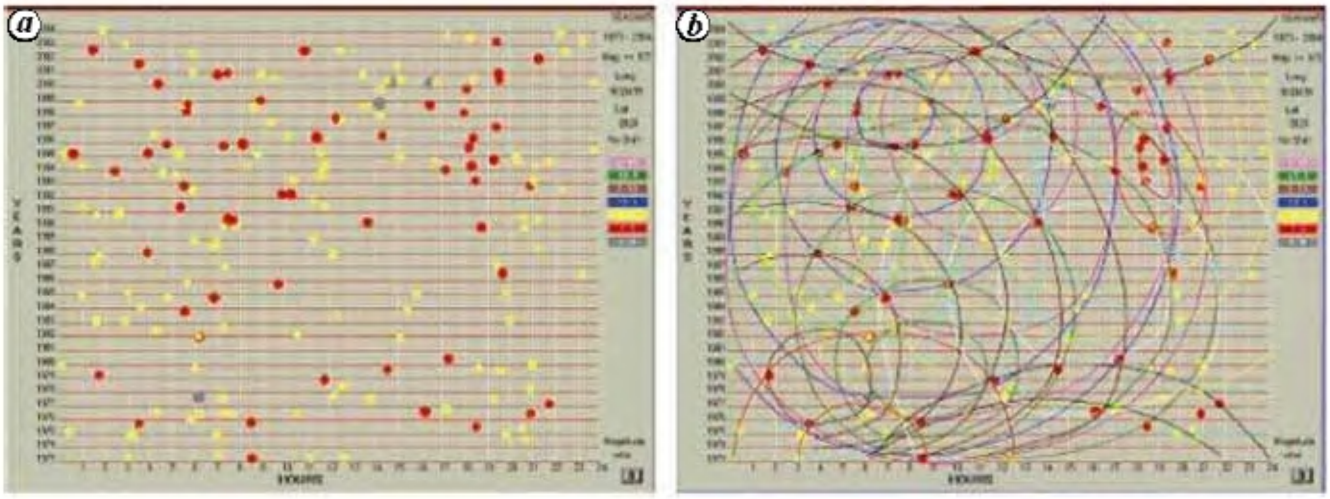

Figure 2. *a*, HE24H of the South East Asia for 32-year period (1973–2004) for earthquakes with magnitude greater than 6.5 (database USGS/NEIC(PDE) 1973 – present). Timings indicated in GMT. *b*, Curve patterns indicating earthquakes through which they are drawn.

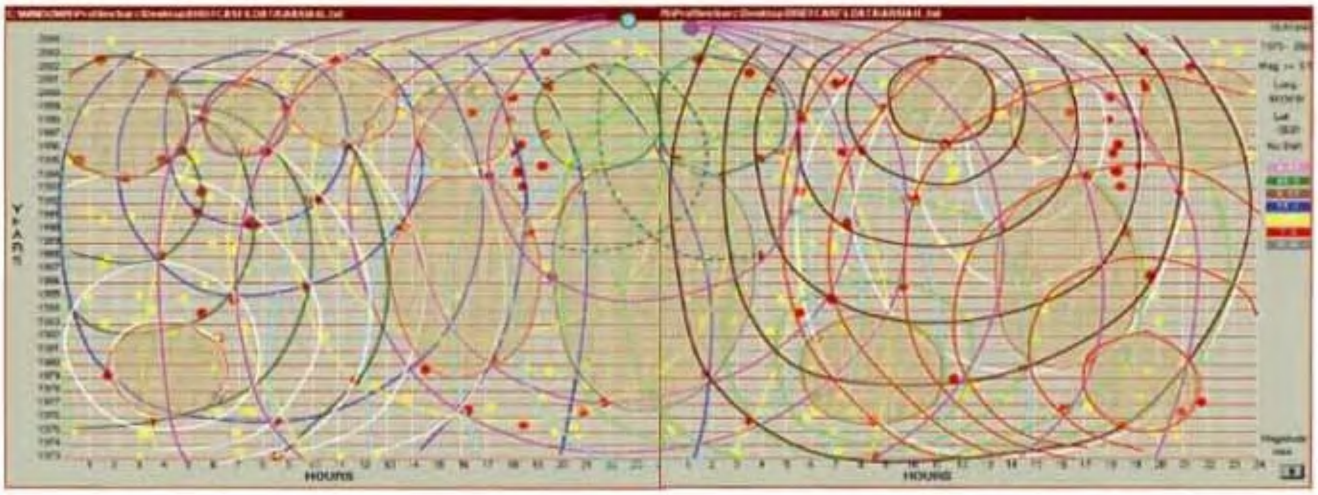

Figure 3. Illustration of two combined histograms (HE24H) of South East Asia for the 32-year period (1973–2004) for earthquakes with magnitude greater than 6.5. Sets of curves similar to Cartesian Oval are shown. All possible eyes of the multiple patterns are also indicated in a semi-opaque shade. Pink colour dot (centre top) represents the great Sumatra earthquake of 26 December 2004. A prominent sky blue colour dot to its left to which many stress fronts converge, could be an impending earthquake in the near future.

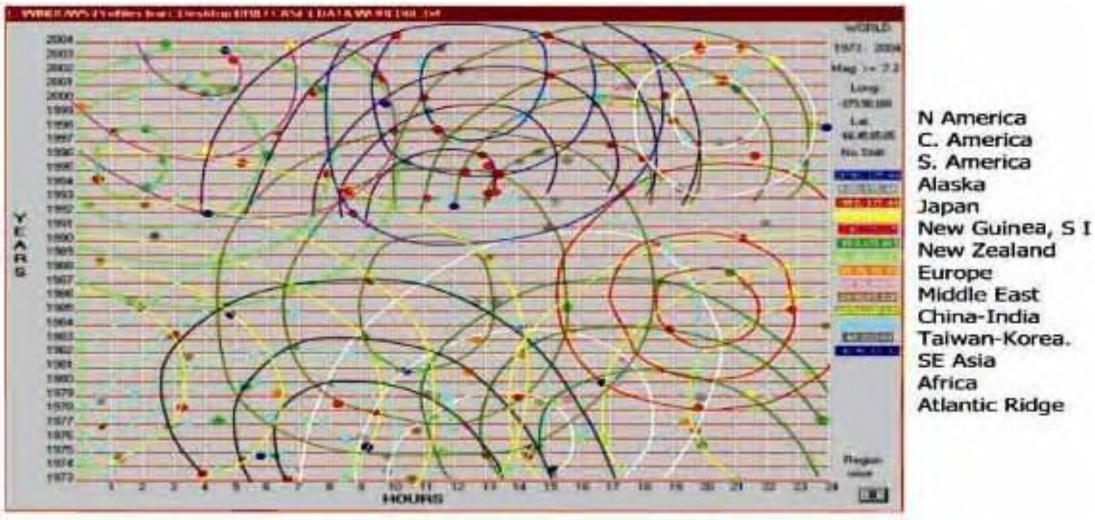

Figure 4. HE24H of the world for the 32-year period (1973–2004) for earthquakes with magnitude greater than 7.2. A set of prominent curves drawn is illustrated. (Databases USGS/NEIC(PDE) 1973 – present)). The pattern with sky blue and yellow colours can be visualized from the raw diagram illustrated in Figure 5, part A.

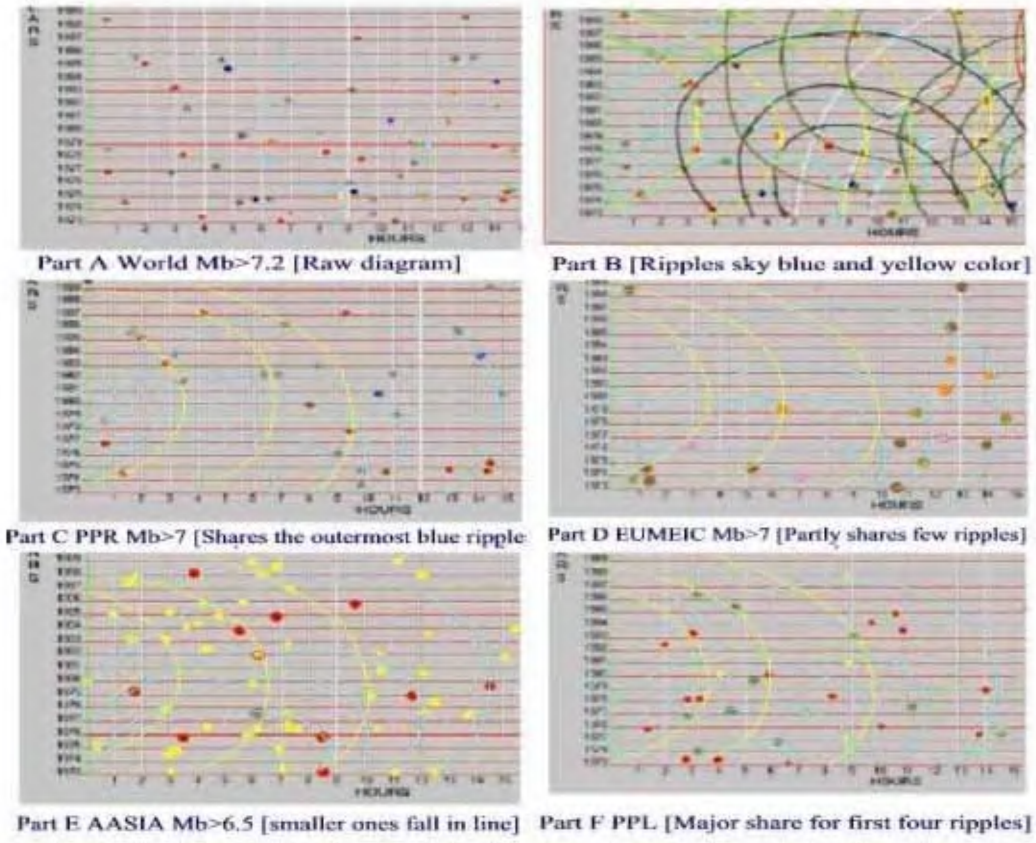

Figure 5. Demonstration of how a global stress front (part B) is shared by different parts of the globe. The set of curves illustrated by sky blue and yellow colours is shared by four major seismically active parts of the globe, as illustrated in the parts C–F.

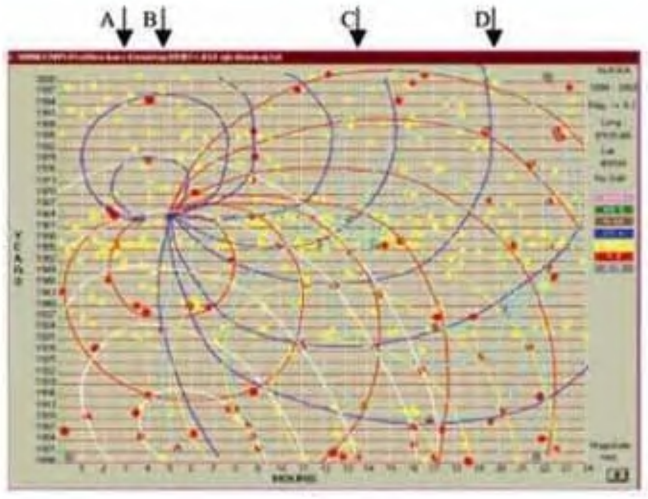

Figure 6. HE24H for Alaska region illustrating how big earthquakes could be formed. Two pairs of earthquakes of magnitude 8+ (indicated by arrows A–D) have multiple stress fronts passing through their point of occurrence. Few of the other types of patterns are also illustrated in white and yellow colours.

There were five earthquakes of magnitude 8 and above, as indicated by arrows and marked with alphabets A–E. The details of these earthquakes are as follows: (A) Onset time of 00 : 33 : 16 on 9 June 1994, *Mb* 8.2. (B) Onset time of 05 : 11 : 23 on 30 July 1995, *Mb* 8.0. (C) Onset time of 13 : 17 : 47 on 19 September 1985, *Mb* 8.1. (D) Onset time of 15 : 35 : 53 on 9 October 1995, *Mb* 8.0. (E) Onset time of 20 : 33 : 14 on 23 June 2001, *Mb* 8.4.

Figure 8 provides multiple stress fronts between three pairs of stronger earthquakes, viz, pairs A–B, C–D, and D–E as indicated by blue, red and green colours respectively.

Between these two types of curves, Cartesian Oval type was mostly constructed when earthquake sets which belonged to a typically vertical section (longitude-dependent) of the globe were considered. Whereas Cardioids type of curves were contributed by all global events and do not indicate any longitude dependency.

Earthquakes that are aligned to provide different curves in HE24H could be possibly caused by stresses of diurnal-type, which were found to be more intense than those of semidiurnal-type. In few such instances, occurrence of the earthquake was not instantaneous and the forces responsible for generating stresses of diurnal-type would make this earthquake-prone area more vulnerable. In this state, semi-diurnal stresses acting on a daily basis take over, and during their application, the region under stress

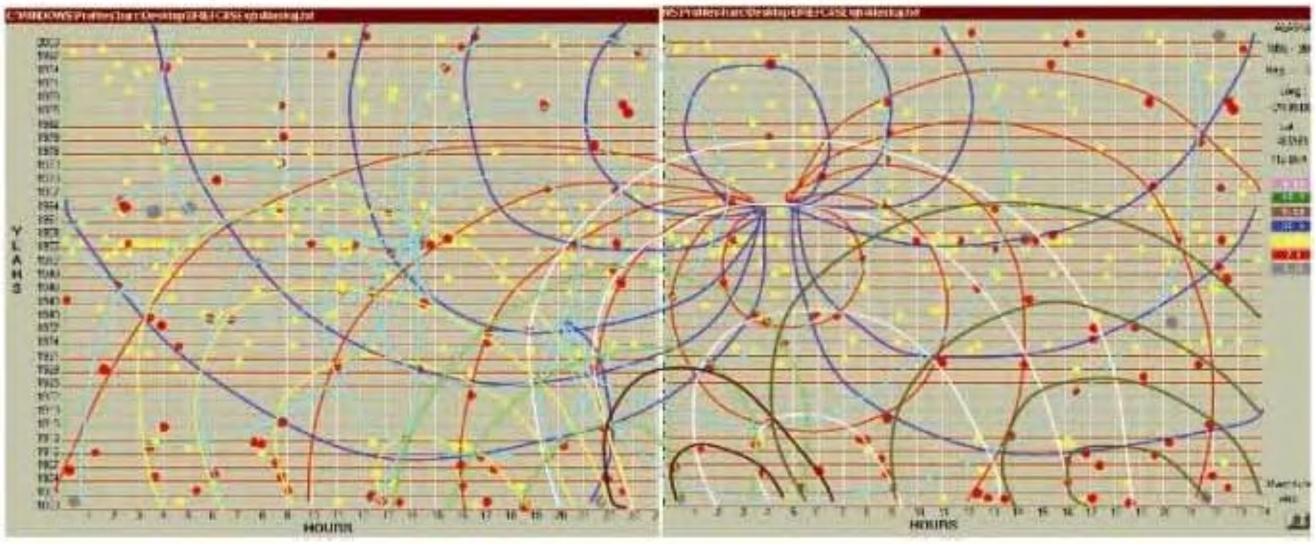

Figure 7. Two histograms (HE24H) of Alaska regions for a 99-year period joined to illustrate extended stress fronts shown in Figure 6 beyond 24 h. As in previous cases, these extended wavefronts fall back within 24 h block.

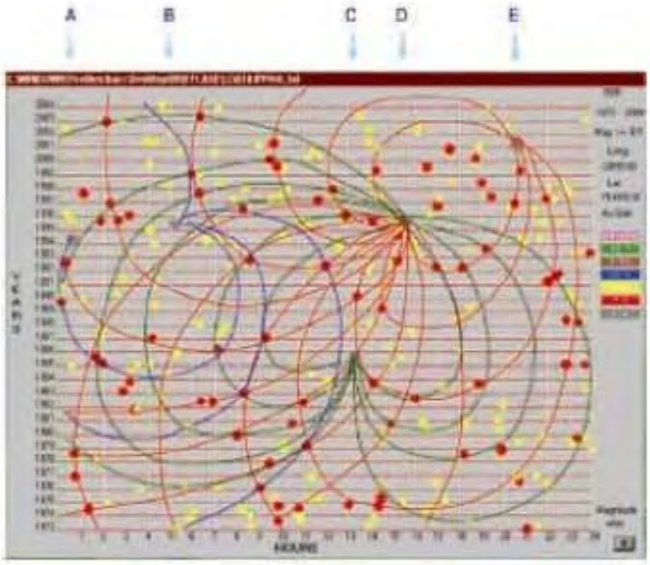

Figure 8. HE24H for PPR (Pacific Plate Right) region for 30-year (1973–2002) period. Multiple stress fronts are seen between three pairs of the stronger earthquakes (Mb = 8 and above) as indicated by different colours.

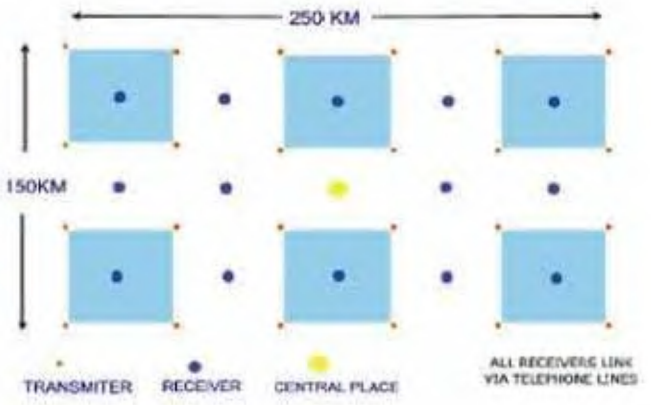

Figure 9. Grid of UHF/VHF links for monitoring high seismicity region.

provides higher emission of the RF noise. The phenomenon continues for few days and subsequently results in the occurrence of earthquakes during the application of one such semidiurnal stress. Regions of many big earthquakes were affected due to diurnal stresses, but they occurred during the application of semidiurnal stresses. The 1960 Chilean earthquake is one such example. Earthquakes of this type may not align any curvature in HE24H.

A grid of UHF/VHF links can be used to monitor the strength of various stress fronts in the seismically active region, which can provide warning for any impending earthquakes. A typical arrangement is illustrated in Figure 9.

A set of four receivers at the location of every blue dot shall receive signals from four transmitters located at four corners of a square of size 50 km × 50 km and operated at different spot frequencies in the UHF/VHF band (Figure 9). The transmission can be through omni directional antenna, since receivers in the adjacent block can also monitor the same signal.

The sensitivity of any commercially available UHF receiver is typically 0.3 μV @ 12 dB SINAD, which is equivalent to –146 dB of input power. Input to four receiver sets operated at different spot frequencies and installed at each blue dot point, can be through different fixed attenuators in the range 10–30 dB (assuming strength of received signals for all four receivers is maintained equal at around –105 dB). The data of signal strength from all receivers can be digitized at low frequency, typically 1–3 Hz, and sent to the central place on telephone lines. The signals from the entire network can thus be monitored centrally.

On a daily basis, the RF noise envelope due to stress front (semidiurnal-type) would rise by about 10–15 dB, which would result in at least one of the receivers (with maximum input attenuation) generating noisy signal. As mentioned earlier and as experienced by the RTSN at Bhatsa net, when the region under observation was under stress and matured for earthquake, it would result in higher levels of RF noise, which can be sensed by the set of four receivers at multiple points. This higher RF noise envelope shall be witnessed (on a daily basis) for few days before the impending earthquake. The envelope of the RF noise caused due to diurnal-type stresses (which is not a daily phenomenon) can also be recorded precisely.

Absolute RF noise measurement in VHF/UHF band can also be carried out with multiple receiver system used in ORSOC[9]. The intensity envelope in the HF band for a few remote radio stations (as in case of the Chilean earthquake sequence) can also be recorded, which should be useful for large area monitoring.

1. Kolvankar, V. G., Nadre, V. N., Arora, S. K. and Rao, D. S., Development and deployment of radio telemetered seismic network at Bhatsa. *Curr. Sci. (Spec. Issue)*, 1992, **62**, 199–212.
2. Kolvankar, V. G., Earthquake sequence of 1991 from Valsad region, Guajrat. BARC-2001/E/006.
3. Ogawa, T., Oike, K. and Miura, T., Electromagnetic radiation from rocks. *J. Geophys. Res.*, 1985, **90**, 6245–6249.
4. Yamada, I., Masuda, K. and Mizutani, H., Electromagnetic and acoustic emission associated with rock fracture. *Phys. Earth Planet. Inter.*, 1989, **57**, 157–168.
5. Warwick, J. W. Stoker, C. and Meyer, T. R., Radio emission associated with rock fracture: Possible application to the Great Chilean earthquake of 22 May 1960. *J. Geophys. Res.*, 1982, **87**, 2851–2859.
6. Lammlein, D. R., Lunar seismicity and tectonics. *Phys. Earth Planet. Inter.*, 1977, **14**, 224–273.
7. Tanaka, S., Ohtake, M. and Sato, H., Evidences for tidal triggering of earthquakes as revealed by the statistical analysis of global data. *J. Geophys. Res.*, 2002, **107**, No. B10, 2211; doi:10.1029/2001 JB001577.
8. Kolvankar, V. G., A study of regional and global earthquake patterns on 24 hour basis. Seismology Division, Bhabha Atomic Research Center, Mumbai, 2005.
9. Takeo, Y. and Ichro, T., Observation of low frequency electromagnetic emissions as precursors to the volcanic eruptions at Mt. Mihara during November 1986. *Phys. Earth Planet. Inter.*, 1989, **57**, 32–39.
10. Gokhberg, M. B., Morgounov, V. A. and Pokhotelov, O. A., *Earthquake Prediction Seismo Electromagnetic Phenomena*, Institute of Earth Physics, Russian Academy of Science, Moscow, Russia, Gorden and Breach, pp. 112–113.
11. Isao, Y., Kuga, K., Tohru, O. and Takashi, A., System for earthquake prediction research in the region of VHF frequency band. *J. Atmos. Electr.*, 2002, **22**, 267–275.
12. Haykawa, M., Molchanov, O. A., Tondoh, and Kawai, E., The precursory signature effect of the Kobe earthquake of VLF subionospheric signals. *J. Commun. Res. Lab.*, 1996, **43**, 169–180.
13. Bulow, R. C., Johnson, C. L. and Shearer, New events discovered in the Apollo Lunar Seismic data. *J. Geophys. Res.*, 2005, **110**, E10003; doi:10.1029/2005 5JE002414.

ACKNOWLEDGEMENTS. I am grateful to NEIC-USGS for providing the earthquake catalogues, Mr Akshay Mittal for help to enhance the resolution of the histograms. I am also grateful to Drs S. K. Kataria, R. S. Chaughule, R. I. K. Moorthy, Falguni Roy, S. M. Sharma and Mr A. M. Patankar for discussions.

Received 20 September 2005; revised accepted 15 May 2007